Three-Dimensional Microfabrication Using Maskless Irradiation with MeV Ion Beams: Proton-Beam Micromachining

Frank Watt, Jeroen A. van Kan, and Thomas Osipowicz

Introduction

As semiconductor device dimensions are scaled down, there is also a parallel trend to miniaturize mechanical components and integrate these micromechanical components with microelectronic devices to form microelectromechanical systems (MEMS). The development of MEMS devices is a high-technology growth area of enormous potential. MEMS devices, which incorporate a combined system of sensors, microprocessors, and actuators, are expected to find applications in a wide range of commercial sectors, ranging from the automotive and aerospace industry, *in situ* process monitoring, and environmental health and safety, to biomedical monitoring and treatment.

The manufacture of micromechanical components requires the development and utilization of novel types of micromachining procedures, and in general, there are a limited number of physical procedures that can be utilized (Figure 1). These include the use of electromagnetic radiation (optical light, ultraviolet light, and x-rays) or charged particle beams [electrons, low-energy heavy ions, and high-energy light ions (e.g., MeV protons)]. Whereas electromagnetic radiation is usually utilized in masked processes (i.e., a selective radiation pattern is transmitted to a resist material through transparent zones in a mask), charged particles are mainly used in a direct-write mode (the particle beam can be focused to a small spot and scanned across the resist material). All of these processes have advantages and disadvantages,[1,2] although at the present time, commercial micromachining technology heavily relies on optical lithography, since it makes sense to capitalize on the major development effort invested in this technique by the microelectronics industry. Although optical lithography is currently the dominant process used for micromachining, and many successful integrated devices have been manufactured (e.g., accelerometers and gyroscopes), this process is essentially a surface technique capable of producing planar devices. It seems likely that, in the future, the scope of micromachining will need to encompass the manufacture of three-dimensional (3D) components and structures.

If we consider the six different physical processes summarized in Figure 1, only two of these processes are capable of true 3D micromachining. X-ray radiation and high-energy protons are the only probes that can significantly penetrate the resist material. Of these two processes, only high-energy proton micromachining has the capability of direct-write 3D micromachining, and this is the subject of this review.

Introduction to High-Energy Proton-Beam Micromachining

It has been known for many years that individual high-energy light ions can produce visually identifiable tracks in resist material, and this phenomenon has been widely used in nuclear and particle physics research for particle detection

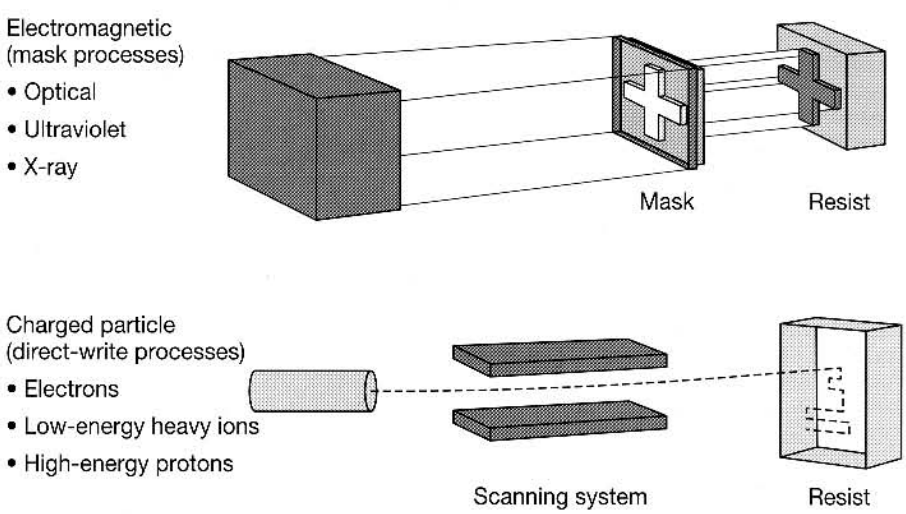

Figure 1. Submicron micromachining processes.

and identification. More recently, heavier ions have been used for lithography,[3] as described in the following article. The first preliminary work on dose exposure requirements using a focused beam of 2-MeV protons in the manufacture of structural lines in poly(methyl methacrylate) (PMMA)[4] was followed by a demonstration of microchannel machining.[5] More recently, it was shown that a scanning focused beam of MeV protons has a high potential for flexible and intricate 3D micromachining.[6–12]

Physical Characteristics of Proton-Beam Micromachining

The path of a high-energy ion (e.g., a 2-MeV proton) in matter is largely determined by electronic collisions, with a smaller contribution from forward elastic nuclear scattering. The ion path can be statistically predicted since the average energy transfer per electron collision is relatively small and many thousands of collisions occur before the ion comes to rest. Using appropriate Monte Carlo techniques, such as the computer code TRIM,[13] the ion path can be traced through matter, and the path of a MeV ion can be characterized by three important features:

- Specific range. The ion penetrates the surface of the sample material and travels through many atomic layers before it comes to rest. The range is therefore relatively high, particularly for high-energy light ions such as protons; for example, 2-MeV protons will penetrate 62 μm into PMMA. Due to the statistical nature of the collision process, the degree of range straggling is small and can be as little as a few percent, for example, the range straggling of 2-MeV protons (range 47 μm) in silicon is approximately 1.6 μm. Ions of the same incident energy therefore travel through material and stop at approximately the same depth. For proton micromachining, a further advantage is that beams of different energies will stop at specific depths in the material.
- Straight path. Since the amount of scattering per collision is small, in general the ion does not suffer large angle collisions and travels in an approximately straight line as it passes into the sample (unlike electrons). A focused MeV proton beam will effectively maintain its spatial resolution as it penetrates the material (except at the end of the range, where there is a significant increase in lateral range straggling). Calculations show that a 2-MeV proton beam traveling through a PMMA film of 5 μm will experience less than a 20-nm spread in the beam profile due to electron collision effects.
- Uniform exposure rate. The exposure rate with depth is relatively uniform (except for a several-fold increase at the end of the range).

These characteristics are specific to proton-beam micromachining and give the process some distinct advantages compared with x-ray lithography. These advantages can be summarized as follows: (a) The focused beam can be directly scanned across the resist, thereby eliminating the need for a mask; (b) the ion beam has a well-defined range in the resist (unlike x-rays) and therefore allows the construction of slots, channels, holes, and so on with well-defined depths; (c) the use of ion beams of different energies enables structures such as slots, channels, and holes to be manufactured with different specific depths; and (d) by changing the angle of the resist with respect to the beam, complex nonprismatic shapes can be machined. In addition, with the advent of a new generation of MeV proton focusing systems, the technology now exists for producing microprobe spot sizes of 100 nm.[14]

Description of the Hardware: Prototype Equipment and Future Requirements

A schematic diagram of a proton micromachining facility is shown in Figure 2. Particle beams from an accelerator are focused to a small spot size and scanned over the sample in a predetermined pattern. At present, proton micromachining is still in its infancy, and customized hardware for proton micromachining has not yet been developed. The early work at the Research Center for Nuclear Microscopy at the National University of Singapore has utilized the existing microprobe,[15] which is located on an HVEE AN2500 Van de Graaff accelerator. Plans are under way in our laboratory, however, to construct a new proton micromachining beam line, based around a state-of-the-art, high-brightness, 3.5-MV single-ended accelerator (HVEE Singletron), a high-excitation quadrupole triplet focusing system, and a customized computer-controlled micromachining target chamber.

Potential Minimum Structure Size

Ultimately, the minimum lateral structure size is determined by the minimum size of the proton beam convoluted with the lateral ionization caused by secondary electrons. Studies have been carried out using Monte Carlo ion-transport calculations coupled with an analytical model for secondary-electron energy deposition.[10] The computer code TRIM[13] was used to calculate the proton trajectories, and a model that describes the radial distribu-

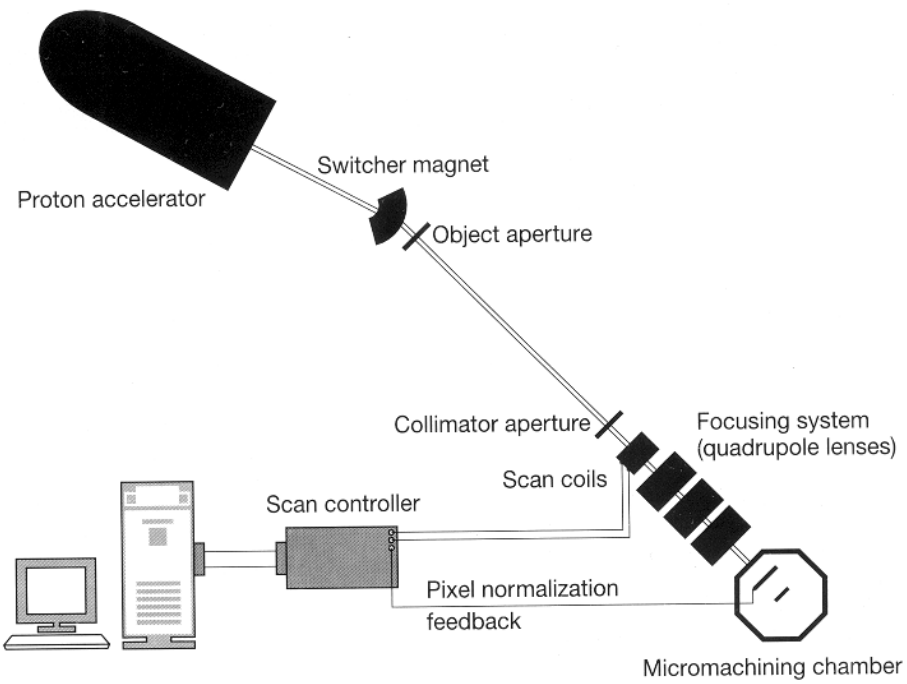

Figure 2. Schematic layout of a proton-beam micromachining system at the Research Center for Nuclear Microscopy, National University of Singapore.

tion of dose around the path of an ion[16,17] was used to determine the spatial energy deposition $D(r)$ around the proton track:

$$D(r) = [K(r) + 1]\frac{Ne^4Z^{*2}}{\alpha m v^2 r}\left[\frac{\left(1 - \frac{r+\theta}{R+\theta}\right)^{1/\alpha}}{r+\theta}\right]. \quad (1)$$

Here Z^* is the effective charge and v is the ion velocity through the resist containing N electrons per cm^3. The electron charge and mass are given by e and m, respectively. R is the maximum range of the δ-rays (i.e., electrons), and r is the distance from the ion track. θ is the range of an electron with specific energy. In our case, the constant $\alpha = 1.667$. Finally, $K(r)$ is a correction to account for the radial dose due to primary events in the region of $r = 1$–10 nm. Results of these calculations show that beyond a depth of about 35 μm, the lateral broadening of the proton beam becomes the dominant factor compared with the effects of secondary-electron energy deposition, which are limited to a maximum lateral dimension of 32 nm at a typical depth of 20 μm for 2.0-MeV and 3.5-MeV protons in resist material. These calculations suggest that there are no physical constraints that would prohibit the future production of sub-100-nm high-aspect-ratio structures.

The practical realization of such structures, however, remains a goal. Factors such as proton-beam size, beam brightness, resist sensitivity and stability, and mechanical stability of the micromachining chamber all play a part in determining the structural feature size. Now, proton-beam sizes of 100 nm can be achieved[14] at beam currents of ~1 pA, so the practical realization of sub-100-nm features should be achievable in the near future.

Dose Exposure Requirements

We have investigated four types of commercial resist materials:[18] the positive resists PMMA, AZP4620, and PMGI; and the negative resist SU8. Of these, AZP4620 proved unsatisfactory, since irradiation with protons may give rise to a combination of both cross-linking and chain-scissioning. Although this resist has a sufficient dose window between positive and negative mode when used with photons, the dose window is not wide enough when high-energy protons are used. The other three resist materials, however, proved satisfactory, with experimentally measured optimum-dose characteristics for high-energy protons as follows: PMMA (60–100 nC/mm^2), PMGI (300 nC/mm^2), and the negative accelerated resist SU8 (10–40 nC/mm^2). At state-of-the-art proton current densities of 1 nA/μm^2, a 1-μm-wide line can be written at a rate of about 10 mm/s in PMMA and 100 mm/s in SU8. This is, of course, still a slow rate of exposure compared with conventional optical and x-ray lithography.

Apart from the end-of-range increase in dose, the dose throughout the proton path is relatively constant. However, we have encountered experimental difficulties in maintaining a constant proton dose per pixel as the beam is digitally scanned across the resist. This is a consequence of variations in the proton current that occur in most accelerator-delivery systems, which in turn stem from variations in the proton-beam energy. The energy stability tends to be worse in belt-driven Van de Graaff accelerators, and when this type of accelerator is utilized, normalization procedures should be employed to provide a constant proton dose per pixel. We have utilized two methods for dose normalization:[18] (1) normalization of the proton dose by monitoring the Rutherford backscattering signal (the scan system moves to the next pixel when a fixed number of proton backscatter counts have been detected); and (2) rapid and repeated scanning, where fluctuations in beam intensity are averaged out. Both methods have been used with varying degrees of success: RBS normalization was found to be more use-

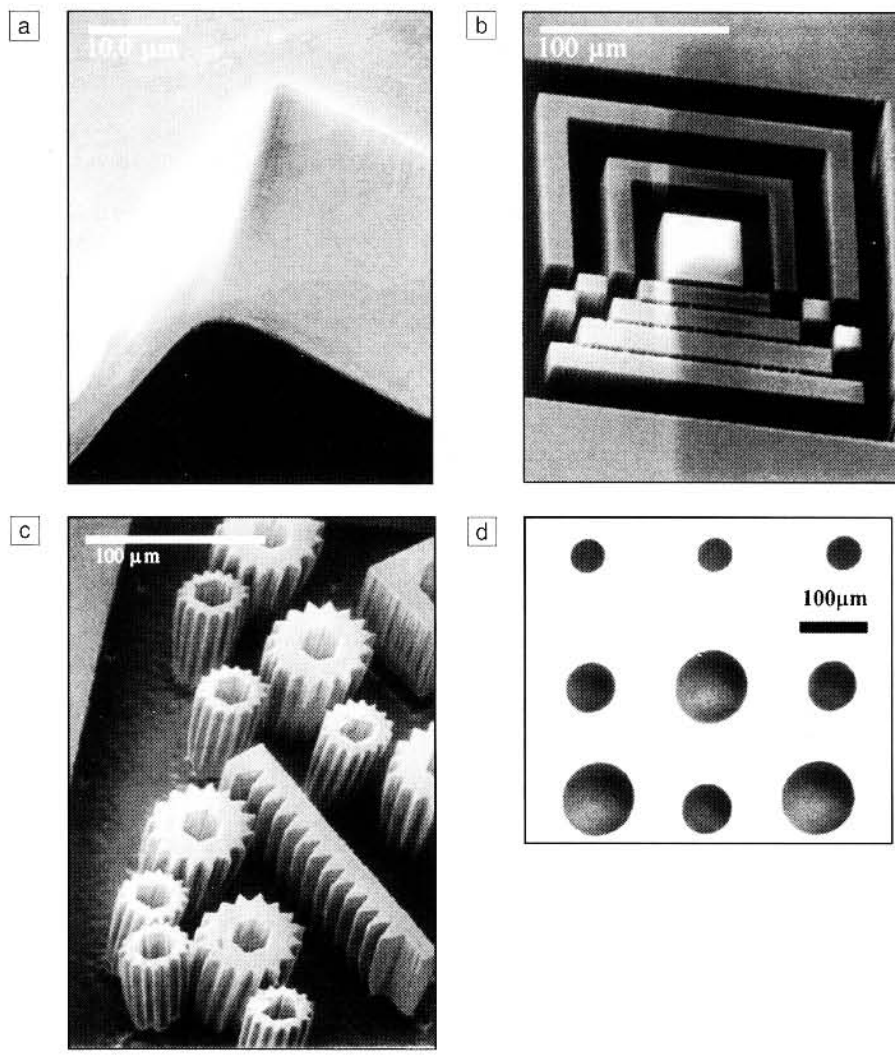

Figure 3. Scanning electron micrographs of single-level structures micromachined in thick poly(methyl methacrylate) (PMMA) using proton-beam micromachining. (a) A corner structure, (b) rectangular slots and ridges, (c) cogs and gear chains, and (d) a bird's-eye view of circular holes. All structures are 62 μm deep. Proton-beam energy was 2 MeV.

ful for the relatively insensitive PMMA and PMGI resists, and rapid scanning was more useful for the more sensitive resist SU8, where the RBS normalization procedure produced insufficient proton-backscatter events per pixel.

Examples of Fabricated Structures

We have investigated the production of test structures in both the positive resist PMMA (where the resist exposed to the proton beam is removed at the development stage) and the negative resist SU8 (where the unexposed resist is removed during development).

Figures 3a–3d show the type of single-level structures that can be machined in PMMA. The electron micrographs depicted here show structures that have been machined using 2-MeV protons in a thick PMMA resist. The 2-MeV protons have a penetration depth of 62 μm, which corresponds to the depth of the resulting machined structures. Figure 3a shows a corner structure with sharp features and smooth walls, and Figure 3b shows the machining of rectangular slots and ridges. Figure 3c shows the type of intricate structures that can be machined using high-resolution scanning, and Figure 3d shows a plan view of machined holes of various selected diameters.

In Figure 4, we see an electron micrograph of the highest-resolution structure so far manufactured using proton micromachining in PMMA. The structure is a narrow line (150 nm wide) produced in a 1-μm-thick layer of PMMA on a silicon substrate using a direct-write 2-MeV proton beam. Due to the lack of customized equipment for proton micromachining, this represents a "first attempt," and it is expected that in the near future, higher resolutions will be achieved.

The type of multilevel structures that can be achieved—in this case, using the negative resist SU8—are shown in Figure 5. Figure 5a shows a two-level "ladder" structure, where the proton beam has been scanned over a thin 36-μm layer of SU8 laid down on a silicon substrate. A 2-MeV proton beam, which penetrates through the resist and into the substrate,

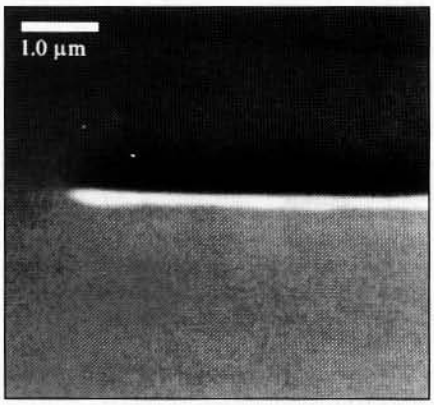

Figure 4. Scanning electron micrograph of a narrow ridge produced by proton-beam micromachining. The ridge is 150 nm wide and 1 nm deep, machined in a thin 1-μm-thick layer of PMMA laid down on a silicon substrate. Proton-beam energy was 2 MeV.

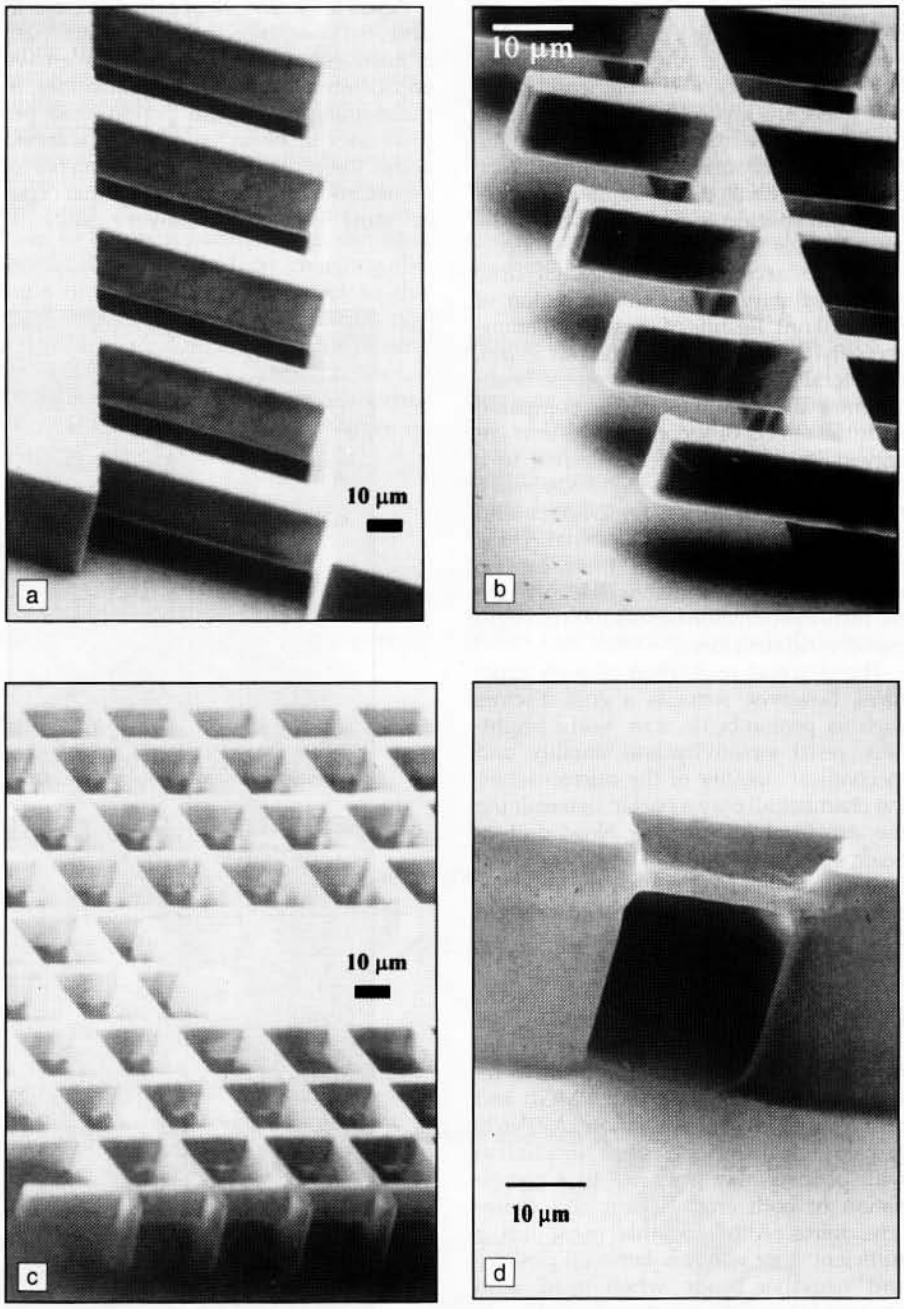

Figure 5. Scanning electron micrographs of multilevel structures in the negative resist SU8, produced by proton-beam micromachining. Structures were made using a single 36-μm layer of SU8 laid down on a silicon substrate. (a) Ladder structure using a 2-MeV proton beam to machine the side anchor supports, and a 1-MeV proton beam to machine the "rungs." (b) Structure showing floating cantilevers. (c) A three-level matrix using 2.0-, 1.0-, and 0.6-MeV protons. (d) A tunnel structure.

has been used to produce the anchor structures (side pieces), and a 1-MeV proton beam, which penetrates only 20 μm and stops in the resist, has been used to produce the "rungs." Figure 5b shows a similar structure made in the same way, but this time incorporating floating cantilever structures. Figure 5c shows an example of a three-level matrix, where the central anchor has been made using 2-MeV protons, and the two-level matrix structure has been made with 0.6- and 1.0-MeV protons. Finally, the same type of multilevel micromachining can be used to fabricate a tunnel structure (Figure 5d). It must be emphasized that all of these test structures have been manufactured using one layer of resist material, thereby demonstrating one of the unique properties of proton micromachining.

Figure 6 shows another novel feature of proton micromachining. Because of the direct-write feature, it is possible to tilt the resist between exposures. Figure 6a shows a two-level structure in SU8, where both exposures have been carried out normal to the resist material. Figure 6b, however, has the shallow (low-energy) structure normal to the proton beam, but the underlying anchor support (higher energy) is at an angle of 40° to the normal.

Concluding Remarks

We have tested the feasibility of a new micromachining technique that has unique characteristics. Proton-beam micromachining is the only direct-write technique capable of true 3D micromachining at the submicron level. Because of the nature of the interaction of protons with matter, a proton beam is able to trace an approximately straight-line path through resist material and stop at a depth that depends on its energy. In addition, the proton beam produces a relatively uniform dose rate along its path. Although these unique characteristics break down somewhat at the end of range, by using a resist layer that is thinner than the penetration depth of the proton beam, end-of-range effects can be avoided where necessary. The well-defined range of the proton beam in the resist allows the production of multilayer structures in a single resist layer, and by tilting the resist between exposures, intricate and angled structures can be produced.

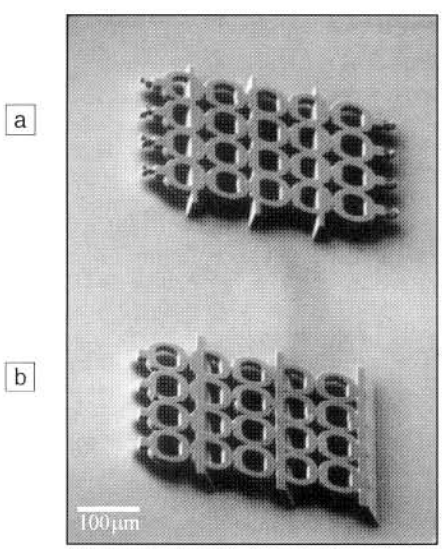

Figure 6. Scanning electron micrograph of two two-level structures in the negative resist SU8, produced by proton-beam micromachining. (a) Exposures carried out normal to the resist material. (b) Underlying anchor support is tilted 40° to the normal.

So far, we have concentrated on the identification of unique properties of proton-beam micromachining and the production of novel and intricate test structures to test the potential of the technique. However, we have also identified niche areas where we believe proton-beam micromachining will have high potential in the future. Since proton-beam micromachining is a direct-write process, it is not as efficient as masked processes such as optical lithography for bulk micromachining, where multiple copies of a structure can be produced in one exposure using multipatterned masks. We recognize this limitation, and have identified four areas which we believe have high potential in the future:

- Stamp and mold manufacture. Proton-beam micromachining has the potential to manufacture individual 3D stamps or molds that can then be used repeatedly for batch and high-volume production. Similar to x-ray lithography, LIGA[19] (the German acronym for lithography, electrodeposition, and molding) electroplating or electroforming of the resist structures can be used to produce metallic molds and stamps. Some of our current projects include development of 3D substrates for tissue engineering,[20] precision molds for integrated-circuit packaging, and microchannels for advanced electrophoresis applications.
- Rapid and cheap prototyping of 3D microstructures. With the rapid expansion in batch production of microcomponents, which invariably involves high capital-equipment expenditure, there is a need for the rapid and efficient development of prototypes. Here there is no need for batch manufacture, since the emphasis is on product research and development rather than mass production. Rapid prototyping is an area in which direct-write processes may have both cost and time advantages.
- Basic research into microstructures. There is a growing need to investigate the properties of microstructures. For example, very little is known about fluid-flow properties in microchannels, friction properties, wear characteristics of moving parts, inertial properties of cantilevers, bioactivity of microimplants, and so on. For basic research purposes, high-volume production is not necessary, and direct-write production of small numbers of custom-built structures may prove highly advantageous.
- Mask production. X-ray lithography (LIGA) is one process that has the potential to manufacture sub-250-nm components for the integrated-circuit industry. The technique, however, requires advanced mask technology: A typical x-ray mask needs to be extremely stable, have sub-250-nm pattern dimensions, and have characteristics such that the pattern is thick enough to block out x-rays in specific regions. The mask thus has to exhibit high-aspect-ratio structures. Proton-beam micromachining has the potential to manufacture such masks.

In conclusion, proton-beam micromachining is a new process that is still in its infancy, but shows a great deal of potential. It has unique characteristics as well as niche commercial applications, and with the advent of new types of high-brightness, high-stability accelerators coupled with advances in high-energy focusing systems, proton-beam micromachining should realize its potential.

References

1. M. Madou, *Fundamentals of Microfabrication* (CRC Press, Boca Raton, FL, 1997).
2. P. Rai Choudury, ed., *Handbook of Microlithography, Micromachining and Microfabrication*, Vol. 1, Monograph PM39 (SPIE—The International Society for Optical Engineering, Bellingham, WA, 1997).
3. B.E. Fischer, *Nucl. Instrum. Methods B* **10/11** (1985) p. 693.
4. M.B.H Breese, G.W. Grime, F. Watt, and D. Williams, *Nucl. Instrum. Methods B* **77** (1993) p. 169.
5. L.M. Mason, A. Roberts, D.N. Jamieson, and A. Saint, in *Ion Beam Modification of Materials*, edited by J.S. Williams, R.G. Elliman, and M.C. Ridgway (Elsevier/North Holland, New York, 1996) p. 1110.
6. F. Watt, *Nucl. Instrum. Methods B* **158** (1999) p. 165.
7. S.V. Springham, T. Osipowicz, J.L. Sanchez, L.H. Gan, and F. Watt, *Nucl. Instrum. Methods B* **130** (1997) p. 155.
8. J.L. Sanchez, J.A. van Kan, T. Osipowicz, S.V. Springham, and F. Watt, *Nucl. Instrum. Methods B* **136–138** (1998) p. 385.

9. D.G. de Kerckhove, M.B.H. Breese, M.A. Marsh, and G.W. Grime, *Nucl. Instrum. Methods B* **136–138** (1998) p. 379.
10. J.A. van Kan, T.C. Sum, T. Osipowicz, and F. Watt, *Nucl. Instrum. Methods B* in press.
11. T. Osipowicz, J.A. van Kan, T.C. Sum, J.L. Sanchez, and F. Watt, *Nucl. Instrum. Methods B* in press.
12. J.A. van Kan, J.L. Sanchez, T. Osipowicz, and F. Watt, in *Proc. HARMST Conf. '99* in press.
13. J.P. Biersack and L.G. Haggmark, *Nucl. Instrum. Methods* **174** (1980) p. 257.
14. F. Watt, T. Osipowicz, T.F. Choo, I. Orlic, and S.M. Tang, *Nucl. Instrum. Methods B* **136–138** (1998) p. 313.
15. F. Watt, *Nucl. Instrum. Methods B* **130** (1997) p. 1.
16. Z. Chunxiang, D.E. Dunn, and R. Katz, *Radiat. Prot. Dosim.* **13** (1985) p. 215.
17. M.P.R. Waligorski, R.N. Hamm, and R. Katz, *Nucl. Tracks Radiat. Meas.* **11** (6) (1986) p. 309.
18. J.A. van Kan, J.L. Sanchez, B. Xu, T. Osipowicz, and F. Watt, *Nucl. Instrum. Methods B* **158** (1999) p. 179.
19. W. Ehrfield and H. Lehr, *Radiat Phys. Chem.* **45** (1995) p. 349.
20. J.L. Sanchez, G. Guy, J.A. van Kan, T. Osipowicz, and F. Watt, *Nucl. Instrum. Methods B* **158** (1999) p. 185. □